Impact of Spin–Orbit Coupling on Photocurrent Generation in Ruthenium Dye-Sensitized Solar Cells

ARTICLE *in* JOURNAL OF PHYSICAL CHEMISTRY LETTERS · JANUARY 2014

Impact Factor: 7.46 · DOI: 10.1021/jz402544r

3 AUTHORS:

Simona Fantacci
Italian National Research Council
93 PUBLICATIONS **6,293** CITATIONS
SEE PROFILE

Enrico Ronca
Princeton University
16 PUBLICATIONS **386** CITATIONS
SEE PROFILE

Filippo De Angelis
Università degli Studi di Perugia
265 PUBLICATIONS **11,207** CITATIONS
SEE PROFILE

THE JOURNAL OF PHYSICAL CHEMISTRY Letters

Letter

pubs.acs.org/JPCL

Impact of Spin–Orbit Coupling on Photocurrent Generation in Ruthenium Dye-Sensitized Solar Cells

Simona Fantacci,*[,†] Enrico Ronca,[†,‡] and Filippo De Angelis*[,†]

[†]Computational Laboratory for Hybrid/Organic Photovoltaics, CNR-ISTM, Via Elce di Sotto 8, I-06123 Perugia, Italy

[‡]Department of Chemistry, University of Perugia, Via Elce di Sotto 8, I-06123 Perugia, Italy

Supporting Information

ABSTRACT: Relativistic TDDFT calculations have been performed employing a novel computational approach to evaluate the impact of spin–orbit coupling (SOC) in the optical and photovoltaic properties of panchromatic Ru^{II} dyes for dye-sensitized solar cells (DSCs). The employed computational setup accurately reproduces the optical properties of the investigated dyes, allowing an assessment of the factors responsible for the varying SOC with the dye metal–ligand environment. While for the prototypical panchromatic black dye sensitizer a negligible SOC effect is found, the SOC-induced spectral broadening calculated for the recently reported DX1 dye partly enhances the light-harvesting efficiency and consequently the photocurrent generation in DSCs based on this dye.

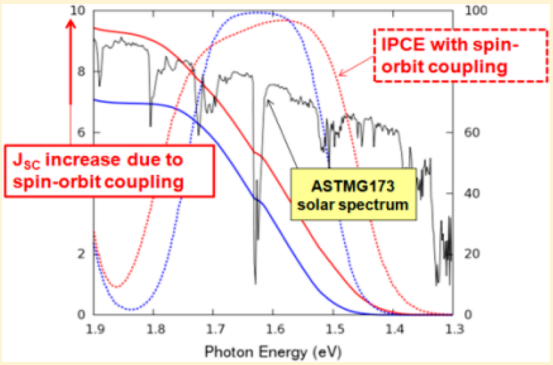

SECTION: Energy Conversion and Storage; Energy and Charge Transport

Over the past decade, Ru-polypyridyl complexes have been demonstrated as versatile and efficient dyes for dye-sensitized solar cells (DSCs).[1] To optimize the matching between the solar radiation and the dye absorption spectrum, new design rules are needed to extend the absorption to the near-infrared (NIR) region.[2−6] Among panchromatic ruthenium dyes, the so-called black dye (BD), [tctpy$(NCS)_3$Ru], tctpy = (4,4′,4″-tricarboxy-2,2′:6,2″-terpyridine), has been widely investigated from both an experimental[2,7−10] and theoretical side[11−16] and tested in DSCs, achieving a record certified efficiency exceeding 11%.[10] Very recently, Kinoshita et al. reported 11.4% efficient tandem DSC devices based on a novel [trans-dichloro-(phenyldimethoxyphosphine)(2,2′;6′,2″-terpyridyl-4,4′,4″-tricarboxylic)Ru] dye,[17] hereafter coded DX1. DX1 showed a BD-like tctpy acceptor ligand (Scheme 1), but compared to BD, it showed enhanced spectral intensity in the 700–900 nm region. This allowed Kinoshita et al. to demonstrate a record short-circuit photocurrent of 26.8 mA/cm^2,[17] comparable to that of conventional silicon-based solar cells. Most notably, the authors of ref 17. attributed the enhanced spectral response to spin-forbidden singlet–triplet transitions, of comparable intensity and spectral position to those characteristic of Os complexes.[3,18−21] This interpretation is quite surprising, considering the large difference in spin–orbit coupling (SOC), which is expected between the second- and third-row Ru and Os centers.[22] Being able to chemically design Ru dyes with Os-like optical properties acting on the ligands of choice will be highly attractive for the large-scale DSCs uptake.

To assess the impact of SOC in ruthenium dyes and its possible implications for photocurrent generation in DSCs, in this Letter, we comparatively investigate the electronic and optical properties of DX1 and BD by means of state-of-the-art scalar relativistic (SR)- and SOC-based time-dependent density functional theory (TDDFT), employing hybrid functionals and continuum solvation models. The study of SOC in ruthenium dyes was pioneered by Daul et al., who 20 years ago calculated the multiplet splitting and SOC in $[Ru(bpy)_3]^{2+}$.[23] Here, we exploit recent advances in SOC-TDDFT, explicitly taking into account the SOC operator in the excited-state TDDFT formalism. The employed computational setup allows us to accurately reproduce the optical properties of both dyes, unraveling at the same time the underlying electronic features responsible for the different BD and DX1 SOC-induced optical response. The impact of SOC on the photocurrent generation in DX1-based DSCs is also modeled, finding a ∼2 mA/cm^2 SOC-induced photocurrent density increase.

We simulate the ground- and excited-state properties of the investigated complexes by the relativistic DFT/TDDFT formalism implemented in the ADF package,[24] based on the zero-order regular approximation (ZORA) two-component Hamiltonian, including the spin–orbit operator in TDDFT.[25−27] SR calculations are also performed as a reference to gauge the explicit impact of SOC on the calculated properties. TDDFT calculations are performed by the B3LYP

Received: November 23, 2013
Accepted: December 29, 2013
Published: December 30, 2013

Scheme 1. Molecular Structures of BD and DX1

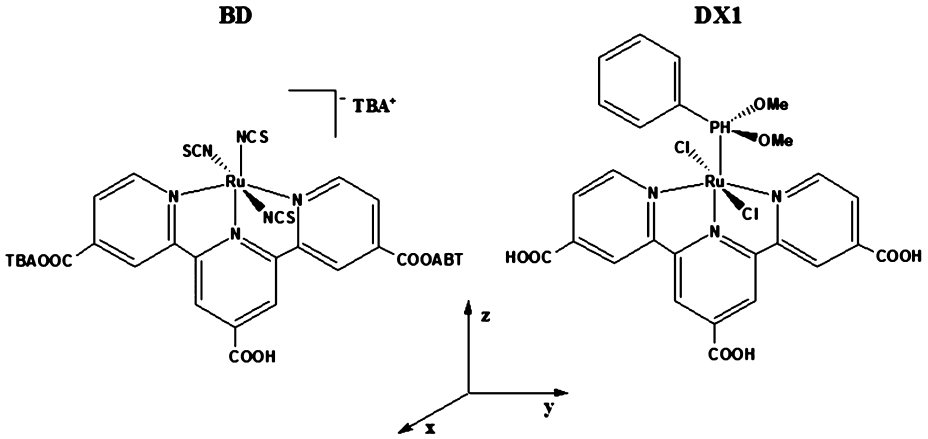

functional on SR-optimized geometries; in all cases, we employ a TZP/DZP basis set; see the Computational Details.

An always-present issue in modeling ruthenium solar cells sensitizers is that of assessing the precise protonation state of these systems.[16,28] BD is typically synthesized as the monoprotonated salt (BD_1H).[2] For comparative purposes, we thus simulated BD_1H and DX1_1H, along with the fully protonated DX1_3H species. The molecular structures of the investigated species are in good agreement with available X-ray data;[2,8] see the Supporting Information.

In Figure 1, we report the comparison between the SR- and SOC-TDDFT simulated spectra of DX1 and BD in acetonitrile, along with the corresponding experimental spectra.[17,29] A small solvatochromic effect was found for DX1_1H by SR-TDDFT, with a ∼0.03 eV spectral blue shift observed from acetonitrile to water solutions; see the Supporting Information. Considering DX1_3H, the SR- and SOC-calculated spectra look quite similar, with a relatively small but appreciable band broadening due to SOC evident at low energy. In agreement with the experimental data, we calculate three main features in the investigated range, at 792, 666, and 495 nm (the last feature showing a pronounced shoulder at 550 nm), to be compared to 792, 620, and 570 nm experimental features.[17] We notice, however, the different intensity ratio calculated for the ∼800 and ∼500 nm features compared to the experimental spectrum and a more pronounced low-energy tail extending above 1000 nm.

Compared to DX1_3H, the mono-protonated DX1_1H shows a slight blue shift of the main visible features (769, 600, 509 nm) and a substantial intensity decrease of the low-energy absorption band, which seems to better match with the experimental spectral shape. It is thus reasonable to speculate that a mixture of different dye protonation states coexists in solution, similarly to what was previously found for the analogous N3 dye.[28] The calculated absorption spectrum for BD_1H is also in good agreement with the experimental one, despite a slight red shift of the low-energy feature (657 versus 620 nm), which induces a slightly different spectral shape compared to the experiment.

To analyze the excited states responsible for the observed phenomenology, we decompose each SOC-calculated transition in terms of the constituting SR-calculated singlet−singlet (S_n) and singlet−triplet (T_n) excitations, Table 1 (we limit this analysis to the ∼800 nm region; see the Supporting Information for the complete data). For DX1_3H, the SR-calculated S_1 (1.538 eV, f = 0.072) and T_2 (1.447 eV, f = 0.000) states (from now on, we switch to eV units, which are convenient to discuss energy differences) are mixed to generate mainly two intense SOC transitions, ST_4 and ST_7, which are found at 1.416 (f = 0.013) and 1.567 (f = 0.058) eV. ST_4 is composed of ∼80% of T_2, while ST_7 is composed of ∼70% of S_1, showing therefore ∼4 times larger intensity than ST4. The two mixed transitions have the same ligand-based arriving state (LUMO, Figure 2) but two different metal-based starting states, HOMO for S_1 and HOMO−1 for T_2 (Figure 2), in line with the expected selection rule for MLCT excitations.[30] A similar picture holds for DX1_1H, although a stronger (∼60/40%) S_1/T_2 mixing is found, producing two SOC states of comparable intensity. The oscillator strength of the SOC states is borrowed from the involved singlet excitations, and as such, the intensity sum of the coupled ST_4 and ST_7 states almost equals the intensity of the original S_1. We stress indeed that *SOC only induces a redistribution of the singlet transitions intensity, not contributing additional transition strength*. In other words, the intensity in the low-energy spectral region is contributed to by the rather intense S_1 transition, which is perturbed by SOC to produce the spectral modifications shown in Figure 1. Along with intensity borrowing, SOC induces a shift in the SR-calculated transitions, which is an estimate of the SOC strength. Furthermore, SOC provides only a small energy downshift (∼0.02 eV) in the lowest excited states (of main triplet character), which, together with the TiO_2 conduction band energy, sets the lowest driving force for electron injection.

Table 1 and Figure 1 show a weaker SOC in the low-energy spectral region for BD_1H compared to that for DX1_1H; ST_4 and ST_7 lie at almost the same energy (within 0.01 eV) as the constituting T_2/S_1 transitions from which they originated, while an energy shift of ∼0.03 and ∼0.05 eV is found for DX1_3H and DX1_1H, respectively, Table 1, in line with the stronger SOC. Furthermore, we notice that BD_1H shows the S_1 transition at a similar energy as DX1_1 (1.574 versus 1.625 eV) but with a reduced oscillator strength (0.013 versus 0.022). This, together with the higher intensity of the main visible band at ∼650 nm, explains the absence of a significant spectral feature at ∼790 nm in BD_1H.

To explain the observed differences with protonation and ligand environment, we resort to a simple approximate one-electron SOC picture. In this framework, the oscillator strength of the SOC state (f_{ST}) is defined by eq 1, and it directly depends on the SOC matrix element, $\langle S_i|H_{so}|T_j\rangle$ and oscillator

dx.doi.org/10.1021/jz402544r | J. Phys. Chem. Lett. 2014, 5, 375−380

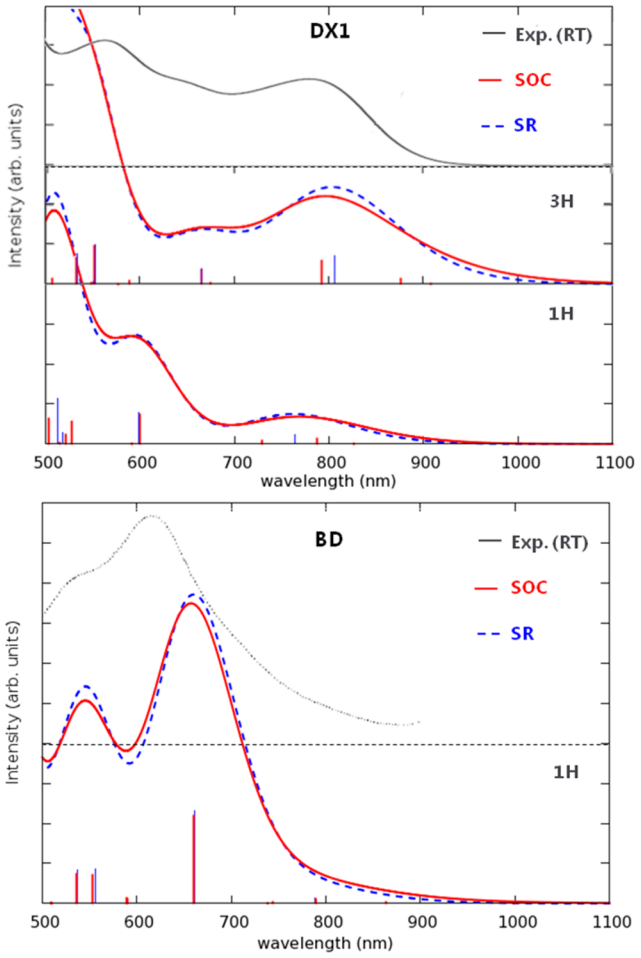

Figure 1. (Upper panel) (Top) Experimental UV−vis spectrum of DX1 in ethanol solution (black solid line), Adapted with permission from ref 17. Copyright 2013 Nature Publishing Group. (Middle) Calculated absorption spectra in acetonitrile for the fully protonated DX1 (DX1_3H) by SR- (blue dashed line) and SOC-TDDFT (red line). (Bottom) Calculated absorption spectra for the monoprotonated DX1 (DX1_1H) by SR- (blue dashed line) and SOC-TDDFT (red line). (Lower panel) (Top) Experimental UV−vis spectrum of BD_1H in ethanol solution (black dashed line). Adapted with permission from ref 29. Copyright 2002 American Chemical Society. Blue (red) vertical lines correspond to SR- (SOC-) calculated unbroadened oscillator strengths. A Gaussian broadening with σ = 0.12 eV (fwhm ≈ 0.3 eV) was used to convolute the calculated transitions. The calculated spectra are on the same scale in the three panels.

strength of the singlet transition (f_S), while it inversely depends on the energy difference of the coupling S_m and T_n states ($E_T - E_S$)

$$f_{ST} = \frac{\langle \varphi_S | H_{SO} | \varphi_T \rangle}{E_T - E_S} f_S \quad (1)$$

For MLCT transitions, the $\langle S_i | H_{so} | T_j \rangle$ matrix element can be qualitatively correlated with the amount of metal character in the orbitals involved in the relevant transitions. Because the involved HOMO and HOMO−1 (Figure 2 and Table 1) show roughly the same metal amount of character, the increased SOC observed in DX1_1H compared to that in DX1_3H is readily explained by the almost resonant energies of the coupling S_1 and T_2 states in the former. Despite the increased

Table 1. Main SOC-Calculated Transitions (eV) and Their Character in Terms of the Constituting SR Transitions and Molecular Orbitals along with the Metal Character of the Involved Molecular Orbitals

DX1_3H			
SOC transitions	SR contribution		SR composition
ST_4 1.416/876 (f = 0.013)	17% S1	1.538 (f = 0.072)	98% (H → L)
	79% T2	1.447 (f = 0.000)	93% (H−1 → L)
ST_7 1.567/791 (f = 0.058)	72% S1	1.538 (f = 0.072)	98% (H → L)
	20% T2	1.447 (f = 0.000)	93% (H−1 → L)
	H−1 (d_{xz})	H (d_{xy})	L (d_{xz})
Ru (%)	52	58	6
DX1_1H			
SOC transitions	SR contribution		SR composition
ST_4 1.577/786 (f = 0.014)	57% S1	1.625 (f = 0.022)	99% (H → L)
	37% T2	1.657 (f = 0.000)	98% (H−1 → L)
ST_7 1.702/729 (f = 0.008)	35% S1	1.625 (f = 0.022)	99% (H → L)
	63% T2	1.657 (f = 0.000)	98% (H−1 → L)
	H−1 (d_{xz})	H (d_{xy})	L (d_{xz})
Ru (%)	52	64	5
BD_1H			
SOC transitions	SR contribution		SR composition
ST_4 1.437/863 (f = 0.003)	95% T2	1.445 (f = 0.000)	96% (H−1 → L)
	3% T3	1.662 (f = 0.000)	93% (H−2 → L)
	1% S1	1.574 (f = 0.013)	97% (H−1 → L)
ST_7 1.572/789 (f = 0.011)	79% S1	1.574 (f = 0.013)	97% (H−1 → L)
	10% T3	1.662 (f = 0.000)	93% (H−2 → L)
	4% T1	1.255 (f = 0.000)	95% (H→ L)
	H−1 (d_{xy})	H (d_{xz})	L (d_{xz})
Ru (%)	40	33	12

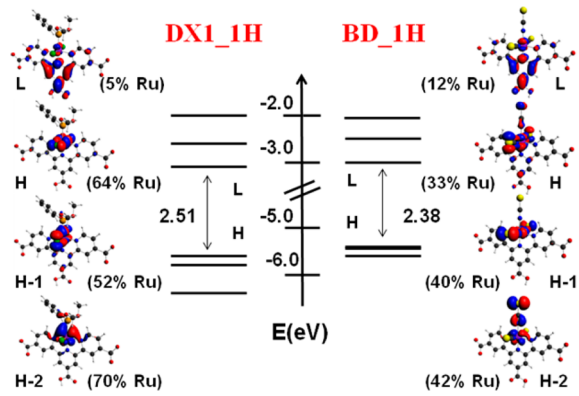

Figure 2. Schematic representation of the frontier orbitals of DX1_1H (right panel) and BD_1H (left panel) calculated by SR-B3LYP. The isodensity plots of the HOMO−2, HOMO−1, HOMO, and LUMO of both dyes are reported along with the related metal character.

SOC, the lower singlet oscillator strength (f_S) penalizes the overall intensity of the SOC transitions in DX1_1H.

dx.doi.org/10.1021/jz402544r | J. Phys. Chem. Lett. 2014, 5, 375−380

The reason for the reduced SOC in BD_1H compared to that in DX1_1H is clearly due to the different electronic structure, whereby the HOMO and HOMO−1 (of d_{xy} and d_{xz} character in DX1_1H) are switched in BD_1H and show a reduced amount of metal character, as previously noted.[17] Because the HOMO−1 is the starting S_1 orbital in BD_1H, coupling with the closely lying T_2, characterized by the same starting orbital, is not allowed.[29] The weak SOC thus originates from indirect coupling to T_3, showing the HOMO−2 (Figure 2) as the starting orbital.

To further quantify the impact of SOC in the calculated optical properties and to compare our calculations with the low-temperature absorption spectrum of the DX1 dye,[17] we report in Figure 3 the DX1_1H absorption spectrum simulated with a reduced broadening (σ = 0.06 eV); see the Supporting Information for the corresponding data for DX1_3H. Our SOC-calculated spectral profile is in good agreement with the low-temperature data, highlighting the two contributions to the spectrum that arise from the ST4 and ST7 SOC excitations; Table 1. On the basis of this data, we also calculated the molar extinction coefficient of DX1_1H, finding a value of 2988 M^{-1} cm^{-1} at 1.58 eV (783 nm), to be compared to the ∼3000 M^{-1} cm^{-1} experimental molar extinction coefficient and to the 1.66 eV (740 nm) experimental absorption maximum at 77 K. Notably, at the SR-TDDFT level, a molar extinction coefficient of 4289 M^{-1} cm^{-1} at 1.63 eV (762 nm) is calculated, Figure 3.

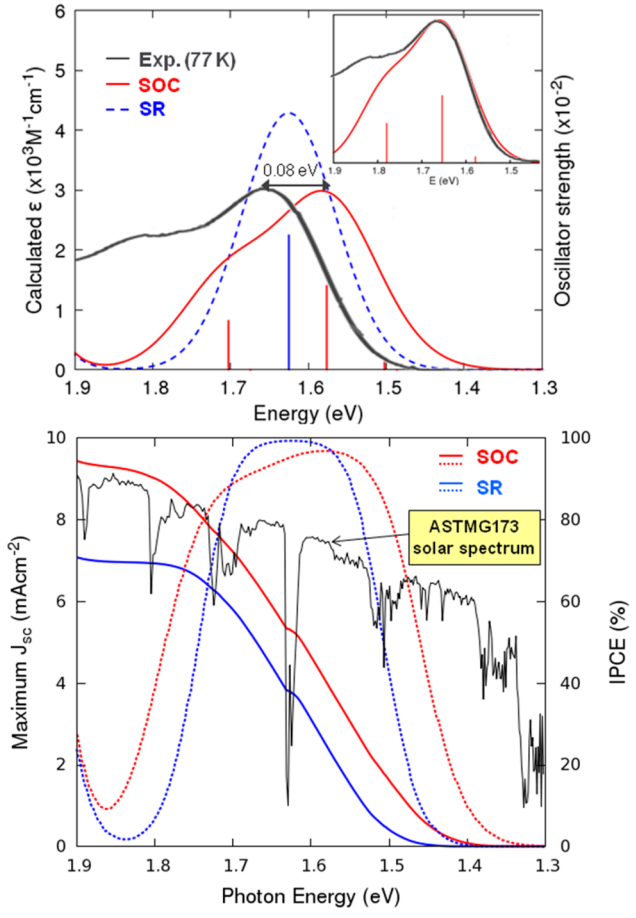

Figure 3. (Top panel) Calculated absorption spectra of DX1_1H by SR (blue dashed line) and SOC (red line) levels of theory, compared with the experimental spectrum (black line) measured at 77 K adapted with permission from ref 17 copyright 2013 Nature Publishing Group. The transitions oscillator strengths are multiplied by 100, and the experimental spectral intensity is rescaled to match the theoretical SOC spectrum. The inset shows the experimental spectrum at 77 K compared to that simulated at the SOC level, red-shifted by 0.08 eV. (Bottom panel) Maximum J_{SC} (mA/cm^2, dotted lines) and IPCE curve (%, full lines) computed at the SR (blue) and SOC (red) levels of theory against the ASTMG173 solar spectrum (black line); see the text for an explanation of the IPCE calculation.

Having the calculated spectra and molar extinction coefficients, we can finally estimate the impact of SOC to the incident photon to current efficiency (IPCE) and photocurrent (J_{SC}) generation due to the lowest absorption band (from 1.3 to 1.9 eV) in DSCs employing the DX1_1H dye. J_{SC} is obtained by integrating the SR- and SOC-calculated absorption spectra against the ASTMG173 solar spectrum (P_{in}):

$$J_{SC}(\mathrm{mA/cm^2}) = \int P_{in}(\mathrm{mW/cm^2}) \times \frac{\lambda}{1240} \times \frac{\mathrm{IPCE}(\lambda)}{100}\, d\lambda \quad (2)$$

The IPCE is defined according to eq 3

$$\mathrm{IPCE} = \mathrm{LHE} \times \phi_{INJ} \times \phi_{COLL} \quad (3)$$

where ϕ_{INJ} is the quantum yield of electron injection and ϕ_{COLL} is the electron collection efficiency. LHE, the light-harvesting efficiency of the photoelectrode, is defined in eq 4

$$\mathrm{LHE}(\lambda) = 1 - 10^{-\alpha(\lambda)d} \quad (4)$$

where $\alpha(\lambda)$ is the reciprocal absorption length, given by the product of the optical absorption cross section or molar extinction coefficient (ε) of the sensitizer and its concentration (C) in the mesoporous film, and d is the thickness of the film.

Our calculations provide us with the wavelength-dependent molar extinction coefficient (see the top of Figure 3), from which the LHE can be calculated knowing the dye concentration in the mesoporous TiO_2 film and the film thickness. We then consider a 10 μm TiO_2 film thickness and a 0.5 M dye concentration in the mesoporous TiO_2 film, which are typical values for mesoporous TiO_2 films and standard ruthenium dyes,[31] and we accordingly calculate LHE(λ). We finally assume that the product of $\phi_{INJ} \times \phi_{COLL}$, that is, the internal quantum efficiency of the device, has the same (unitary) value both in the SR and SOC cases to calculate IPCE(λ).

The obtained results are reported in Figure 3, which clearly highlight how SOC sizably contributes to enhanced J_{SC} generation in DX1-based DSCs, despite the reduced molar extinction coefficient at the absorption maximum compared to SR-calculated data. It is worth noting that *the main SOC effect is that of broadening the IPCE curves rather than providing additional IPCE features*. This is due to the spectral broadening of Figure 3, which contributes an overall J_{SC} gain from 7.1 to 9.4 mA/cm^2 in the considered low-energy region. Notice that the estimated 2.3 mA/cm^2 J_{SC} increase, although sizable, is quite small compared to the overall 26.8 mA/cm^2 J_{SC} measured for DX1-based DSCs.[17]

In summary, we have reported the first SOC-TDDFT on the optical properties of ruthenium solar cell sensitizers. Our calculations have allowed us to quantitatively evaluate the impact of SOC in the optical and photovoltaic properties of prototypical panchromatic ruthenium dyes. The DX1 low-lying spectral feature originates from the presence of a rather intense single−singlet excitation, which is moderately perturbed by the

dx.doi.org/10.1021/jz402544r | J. Phys. Chem. Lett. 2014, 5, 375−380

nearby singlet−triplet excitations by SOC. Despite the relatively small impact of SOC in the position of the calculated absorption maxima (∼0.05 eV), the SOC-induced spectral broadening slightly enhances the light-harvesting efficiency, and it consequently contributes additional photocurrent (∼2 mA/cm^2) in DX1-sensitized DSCs. The employed computational approach constitutes the interpretative basis and computational framework for a quantitative evaluation of SOC in related metallorganic solar cell sensitizers.

EXPERIMENTAL METHODS

Computational Details. The Amsterdam density functional program package in its latest version (ADF2013) has been used for all calculations.[24,32,33] The molecular geometries of all of the investigated complexes were optimized in the gas phase employing the BP exchange−correlation functional (including the Vosko−Wilk−Nusair[34] LDA parametrization and Becke[35] and Perdew[36] gradient corrections to the exchange and correlation, respectively) and using the ZORA TZP basis set[37] for the metal atoms (the cores 1s−3d for ruthenium were kept frozen) and the ZORA DZP for the lighter elements (the 1s core for carbon, nitrogen, and oxygen and 1s−2p for sulfur were kept frozen).[37] In the geometry optimization, the relativistic effects were taken into account through the ZORA Hamiltonian in its scalar approximation as implemented in the ADF code.[38] TDDFT calculations have been performed on the BP geometries using the B3LYP (including the Vosko−Wilk−Nusair[34] LDA parametrization and 20% HF exchange)[39] exchange−correlation functional. The relativistic TDDFT formalism implemented in ADF for closed-shell molecules, including SOC, is based on the ZORA two-component Hamiltonian.[25,40] Relativistic spectra have been evaluated taking into account the SR effects by computing both singlet−singlet and singlet−triplet excited states and by including the SOC in a self-consistent perturbative way.[27] Each SO transition is then related to the corresponding scalar one and can be expressed as the combination of the singlet−singlet and singlet−triplet excitations. In the calculations of the spectra, we have taken into account the 50−60 lowest singlet−singlet and singlet−triplet transitions. Solvation effects were included in both TDDFT relativistic and nonrelativistic calculations by the "Conductor-like Screening Model" (COSMO)[41] of solvation as implemented in the ADF code. The absorption spectra have been simulated by interpolating the computed transitions by Gaussian functions with σ = 0.12 and 0.06 eV.

ASSOCIATED CONTENT

Supporting Information

Optimized molecular structures along with the main optimized geometrical parameters of DX1_3H, DX1_1H, and BD_1H. Energy and character of the frontier orbitals of DX1_3H, DX1_1H, and BD_1H. Main SOC-TDDFT transitions of DX1_3H, DX1_1H, and BD_1H. Computed SR- and SOC-TDDFT spectra of DX1_3H in the eV scale. This material is available free of charge via the Internet at http://pubs.acs.org.

AUTHOR INFORMATION

Corresponding Authors

*E-mail: simona@thch.unipg.it (S.F.).
*E-mail: filippo@thch.unipg.it (F.D.A.).

Notes

The authors declare no competing financial interest.

ACKNOWLEDGMENTS

We thank MIUR-PRIN-2010 and FP7-ENERGY-2010 261920 "ESCORT" for financial support.

REFERENCES

(1) O'Regan, B.; Grätzel, M. A Low-Cost, High-Efficiency Solar Cell Based on Dye-Sensitized Colloidal TiO_2 Films. *Nature* **1991**, *353*, 737.
(2) Nazeeruddin, M. K.; Péchy, P.; Renouard, T.; Zakeeruddin, S. M.; Humphry-Baker, R.; Comte, P.; Liska, P.; Cevey, L.; Costa, E.; Shklover, V.; et al. Engineering of Efficient Panchromatic Sensitizers for Nanocrystalline TiO_2-Based Solar Cells. *J. Am. Chem. Soc.* **2001**, *123*, 1613−1624.
(3) Altobello, S.; Argazzi, R.; Caramori, S.; Contado, C.; Da Fré, S.; Rubino, P.; Choné, C.; Larramona, G.; Bignozzi, C. A. Sensitization of Nanocrystalline TiO_2 with Black Absorbers Based on Os and Ru Polypyridine Complexes. *J. Am. Chem. Soc.* **2005**, *127*, 15342−15343.
(4) Abbotto, A.; Sauvage, F.; Barolo, C.; De Angelis, F.; Fantacci, S.; Graetzel, M.; Manfredi, N.; Marinzi, C.; Nazeeruddin, M. K. Panchromatic Ruthenium Sensitizer Based on Electron-Rich Heteroarylvinylene π-Conjugated Quaterpyridine for Dye-Sensitized Solar Cells. *Dalton Trans.* **2011**, *40*, 234−242.
(5) Kinoshita, T.; Fujisawa, J.-i.; Nakazaki, J.; Uchida, S.; Kubo, T.; Segawa, H. Enhancement of Near-IR Photoelectric Conversion in Dye-Sensitized Solar Cells Using an Osmium Sensitizer with Strong Spin-Forbidden Transition. *J. Phys. Chem. Lett.* **2012**, *3*, 394−398.
(6) Chou, C.-C.; Wu, K.-L.; Chi, Y.; Hu, W.-P.; Yu, S. J.; Lee, G.-H.; Lin, C.-L.; Chou, P.-T. Ruthenium(II) Sensitizers with Heteroleptic Tridentate Chelates for Dye-Sensitized Solar Cells. *Angew. Chem., Int. Ed.* **2011**, *50*, 2054.
(7) Nazeeruddin, M. K.; Pechy, P.; Gratzel, M. Efficient Panchromatic Sensitization of Nanocrystalline TiO_2 Films by a Black Dye Based on a Trithiocyanato-Ruthenium Complex. *Chem. Commun.* **1997**, 1705−1706.
(8) Shklover, V.; Nazeeruddin, M. K.; Grätzel, M.; Ovchinnikov, Y. E. Packing of Ruthenium Sensitizer Molecules on Mostly Exposed Faces of Nanocrystalline TiO_2: Crystal Structure of $(NBu^{4+})_2[Ru(H_2tctterpy)(NCS)_3]^{2-}$·0.5DMSO. *Appl. Organomet. Chem.* **2002**, *16*, 635−642.
(9) Srimath Kandada, A. R.; Fantacci, S.; Guarnera, S.; Polli, D.; Lanzani, G.; De Angelis, F.; Petrozza, A. Role of Hot Singlet Excited States in Charge Generation at the Black Dye/TiO_2 Interface. *ACS Appl. Mater. Inter.* **2013**, *5*, 4334−4339.
(10) Han, L.; Islam, A.; Chen, H.; Malapaka, C.; Chiranjeevi, B.; Zhang, S.; Yang, X.; Yanagida, M. High-Efficiency Dye-Sensitized Solar Cell with a Novel Co-Adsorbent. *Energy Environ. Sci.* **2012**, *5*, 6057−6060.
(11) Aiga, F.; Tada, T. Molecular and Electronic Structures of Black Dye; an Efficient Sensitizing Dye for Nanocrystalline TiO_2 Solar Cells. *J. Mol. Struct.* **2003**, *658*, 25.
(12) Ghosh, S.; Chaitanya, G. K.; Bhanuprakash, K.; Nazeeruddin, M. K.; Grätzel, M.; Yella, R. P. Electronic Structures and Absorption Spectra of Linkage Isomers of Trithiocyanato (4,4′,4″-Tricarboxy-2,2′:6,2″-terpyridine) Ruthenium(II) Complexes: A DFT Study. *Inorg. Chem.* **2006**, *45*, 7600.
(13) Li, M.-X.; Zhang, H.-X.; Zhou, X.; Pan, Q.-J.; Fu, H.-G.; Sun, C.-C. Theoretical Studies of the Electronic Structure and Spectroscopic Properties of$[Ru(Htcterpy)(NCS)_3]^{3-}$. *Eur. J. Inorg. Chem.* **2007**, 2171.
(14) Govindasamy, A.; Chen, L.; Tsuboi, H.; Koyama, M.; Endou, A.; Takaba, H.; Kubo, M.; Del Carpio, C. A.; Miyamoto, A. Theoretical Investigation of the Photophysical Properties of Black Dye Sensitizer-[(H3-tctpy)M(NCS)3] (M = Fe, Ru, Os) in Dye Sensitized Solar Cells. *Jpn. J. Appl. Phys.* **2007**, *46*, 2655.
(15) Li, M.-X.; Zhou, X.; Xia, B.-H.; Zhang, H.-X.; Pan, Q.-J.; Liu, T.; Fu, H.-G.; Sun, C.-C. Theoretical Studies on Structures and Spectroscopic Properties of Photoelectrochemical Cell Ruthenium Sensitizers, $[Ru(H_mtcterpy)(NCS)_3]^{n-}$ (m = 0, 1, 2, and 3; n = 4, 3, 2, and 1). *Inorg. Chem.* **2008**, *47*, 2312.

(16) Fantacci, S.; Lobello, M. G.; De Angelis, F. Everything You Always Wanted to Know About Black Dye (but Were Afraid to Ask): A DFT/TDDFT Investigation. *Chimia* **2013**, *67*, 121−128.
(17) Kinoshita, T.; Dy, J. T.; Uchida, S.; Kubo, T.; Segawa, H. Wideband Dye-Sensitized Solar Cells Employing a Phosphine-Coordinated Ruthenium Sensitizer. *Nat. Photonics* **2013**, *7*, 535−539.
(18) Sauvé, G.; Cass, M. E.; Coia, G.; Doig, S. J.; Lauermann, I.; Pomykal, K. E.; Lewis, N. S. Dye Sensitization of Nanocrystalline Titanium Dioxide with Osmium and Ruthenium Polypyridyl Complexes. *J. Phys. Chem. B* **2000**, *104*, 6821−6836.
(19) Kumaresan, D.; Shankar, K.; Vaidya, S.; Schmehl, R. H. Photochemistry and Photophysics of Coordination Compounds: Osmium. *Top. Curr. Chem.* **2007**, *281*, 101−142.
(20) Alebbi, M.; Bignozzi, C. A.; Heimer, T. A.; Hasselmann, G. M.; Meyer, G. J. The Limiting Role of Iodide Oxidation in *cis*-$Os(dcb)_2(CN)_2/TiO_2$ Photoelectrochemical Cells. *J. Phys. Chem. B* **1998**, *102*, 7577−7581.
(21) Yamaguchi, T.; Miyabe, T.; Ono, T.; Arakawa, H. Synthesis of Novel β-Diketonate Bis(bipyridyl) Os(II) Dyes for Utilization of Infrared Light in Dye-Sensitized Solar Cells. *Chem. Commun.* **2010**, *46*, 5802−5804.
(22) Solomon, E. I.; Lever, A. B. P. *Inorganic Electronic Structure and Spectroscopy*; John Wiley & Sons, Inc.: Hoboken, NJ, 1999; Vol. *1*.
(23) Daul, C.; Baerends, E. J.; Vernooijs, P. A Density Functional Study of the MLCT States of $[Ru(bpy)_3]^{2+}$ in D_3 Symmetry. *Inorg. Chem.* **1994**, *33*, 3538−3543.
(24) te Velde, G.; Bickelhaupt, F. M.; Baerends, E. J.; Fonseca Guerra, C.; van Gisbergen, S. J. A.; Snijders, J. G.; Ziegler, T. Chemistry with ADF. *J. Comput. Chem.* **2001**, *22*, 931−967.
(25) Visscher, L.; van Lenthe, E. On the Distinction Between Scalar and Spin−Orbit Relativistic Effects. *Chem. Phys. Lett.* **1999**, *306*, 357−365.
(26) Wang, F.; Ziegler, T. Theoretical Study of the Electronic Spectra of Square-Planar Platinum(II) Complexes Based on the Two-Component Relativistic Time-Dependent Density-Functional Theory. *J. Chem. Phys.* **2005**, *123*, 194102/1−194102/10.
(27) Wang, F.; Ziegler, T. A Simplified Relativistic Time-Dependent Density-Functional Theory Formalism for the Calculations of Excitation Energies Including Spin−Orbit Coupling Effect. *J. Chem. Phys.* **2005**, *123*, 154102−154110.
(28) Pizzoli, G.; Lobello, M. G.; Carlotti, B.; Elisei, F.; Nazeeruddin, M. K.; Vitillaro, G.; De Angelis, F. Acid−Base Properties of the N3 Ruthenium(II) Solar Cell Sensitizer: A Combined Experimental and Computational Analysis. *Dalton Trans.* **2012**, *41*, 11841.
(29) Bauer, C.; Boschloo, G.; Mukhtar, E.; Hagfeldt, A. Interfacial Electron-Transfer Dynamics in $Ru(tcterpy)(NCS)_3$-Sensitized TiO_2 Nanocrystalline Solar Cells. *J. Phys. Chem. B* **2002**, *106*, 12693−12704.
(30) Baková, R.; Chergui, M.; Daniel, C.; Vlček, A., Jr.; Záliš, S. Relativistic Effects in Spectroscopy and Photophysics of Heavy-Metal Complexes Illustrated by Spin−Orbit Calculations of $[Re(imidazole)(CO)_3(phen)]+$. *Coord. Chem. Rev.* **2011**, *255*, 975−989.
(31) Dell'Orto, E.; Raimondo, L.; Sassella, A.; Abbotto, A. Dye-Sensitized Solar Cells: Spectroscopic Evaluation of Dye Loading on TiO_2. *J. Mater. Chem.* **2012**, *22*, 11364−11369.
(32) ADF2012. *SCM, Theoretical Chemistry*. Vrije Universiteit: Amsterdam, The Netherlands, http://www.scm.com (2013).
(33) Fonseca Guerra, C.; Snijders, J. G.; te Velde, G.; Baerends, E. J. Towards an Order-N DFT Method. *Theor. Chem. Acc.* **1998**, *99*, 391−403.
(34) Vosko, S. H.; Wilk, L.; Nusair, M. Accurate Spin-Dependent Electron Liquid Correlation Energies for Local Spin Density Calculations: A Critical Analysis. *Can. J. Phys.* **1980**, *58*, 1200−1211.
(35) Becke, A. D. Density-Functional Exchange-Energy Approximation with Correct Asymptotic Behavior. *Phys. Rev. A* **1988**, *38*, 3098−3100.
(36) Perdew, J. P. Density-Functional Approximation for the Correlation Energy of the Inhomogeneous Electron Gas. *Phys. Rev. B* **1986**, *33*, 8822−8824.
(37) Van Lenthe, E.; Baerends, E. J. Optimized Slater-Type Basis Sets for the Elements 1−118. *J. Comput. Chem.* **2003**, *24*, 1142−1156.
(38) van Lenthe, E.; Ehlers, A.; Baerends, E.-J. Geometry Optimizations in the Zero Order Regular Approximation for Relativistic Effects. *J. Chem. Phys.* **1999**, *110*, 8943−8953.
(39) Stephens, P. J.; Devlin, F. J.; Chabalowski, C. F.; Frisch, M. J. Ab Initio Calculation of Vibrational Absorption and Circular Dichroism Spectra Using Density Functional Force Fields. *J. Phys. Chem.* **1994**, *98*, 11623−11627.
(40) van Lenthe, E.; Baerends, E. J.; Snijders, J. G. Relativistic Regular Two-Component Hamiltonians. *J. Chem. Phys.* **1993**, *99*, 4597−4610.
(41) Pye, C. C.; Ziegler, T. An Implementation of the Conductor-Like Screening Model of Solvation within the Amsterdam Density Functional Package. *Theor. Chem. Acc.* **1999**, *101*, 396−408.